PAPER

Ultrafast domain wall propagation due to the interfacial Dzyaloshinskii–Moriya interaction

IOP Publishing Nanotechnology
Nanotechnology 31 (2020) 125707 (6pp) https://doi.org/10.1088/1361-6528/ab5f83

Ultrafast domain wall propagation due to the interfacial Dzyaloshinskii–Moriya interaction

D Mancilla-Almonacid[1], R Jaeschke-Ubiergo[2], A S Núñez[2] and S Allende[1]

[1] Departamento de Física, CEDENNA, Universidad de Santiago de Chile, USACH, Av. Ecuador 3493, Santiago, Chile
[2] Departamento de Física, CEDENNA, Facultad de Ciencias Físicas y Matemáticas, Universidad de Chile, Av. Blanco Encalada 2008, Santiago, Chile

E-mail: sebastian.allende@usach.cl

Received 11 June 2019, revised 30 October 2019
Accepted for publication 6 December 2019
Published 8 January 2020

Abstract

It is shown that the interplay between curvature and interfacial Dzyalonshinsky–Moriya interaction (DMI) is a pathway to ultrafast domain wall (DW) dynamics in ferromagnetic nanotubes. In this work, we theoretically study the effect that interfacial DMI has on the average velocity of a vortex DW in thin ferromagnetic nanotubes grown around a core composed of heavy atoms. Our main result shows that by delaying the Walker breakdown instability, the DW average velocity is of the order of 10^3 m s^{-1}, which is greater than usual values for these systems. The remarkable velocities achieved through this configuration could greatly benefit the development of spintronic devices.

Supplementary material for this article is available online

Keywords: domain wall motion, magnetic nanotubes, Dzyalonshinsky–Moriya interaction

(Some figures may appear in colour only in the online journal)

1. Introduction

The exploration of the dynamical properties of curved ferromagnetic systems has become a fertile ground for potential applications in spintronic devices such as memory devices and microwave technologies, among others [1–3]. The reason to focus on these structures is that the curvature induces anisotropies and chiral effects that arise from the lack of collinearity of the spin moments. Effects such as the effective anisotropy and antisymmetric exchange, i.e. Dzyaloshinskii–Moriya-like interaction, emerge in a phenomenological sense regardless of the details of the underlying crystal structure [1, 2, 4]. In this sense, the curvature becomes a new element in the toolkit of magnetization control and related phenomena. It has been shown that curvature effects can affect the magnetic properties of the structures, altering dramatically the basic picture of texture dynamics, such as spin waves [5], domain walls (DWs) motion [6–9], and skyrmions related phenomena [10, 11].

Among the several ferromagnetic curved nanostructures, nanotubes stand out over the other nanostructures due to the ultrafast DW motion against the usual DW motion given in magnetic stripes [12, 9]. Also, nanotubes present a chiral symmetry breaking in the DW motion [13]. These properties allow nanotubes to be an excellent candidate for various magnetic devices [9].

Ferromagnetic nanotubes present a Dzyaloshinskii–Moriya-like interaction that arises from their curvature. This induces a chiral symmetry breaking in the DW dynamics. An interesting competition is expected if the system is engineered to display an actual Dzyaloshinskii–Moriya interaction (DMI) as well. This type of exchange has been included in systems with ultrathin magnetic films for the study of the DW motion [14–16]. For example, Thiaville *et al* observed DW motion with large velocities under large fields at stationary conditions [14]. In nanotubes, Goussev *et al* studied bulk Dzyaloshinskii–Moriya DWs in magnetic nanotubes with non-radial component in the magnetization [17]. They observed a dependence of the DW velocity with the chirality and the DMI. In this context, fabricating ferromagnetic nanotubes with DMI could be possible by using atomic layer deposition [18, 19]. Therefore, a theoretical study of DW motion in

ferromagnetic nanotubes with interfacial DMI must be done if we want to understand the physics of these systems.

In this work, we studied the effect that DMI has on the average velocity of the DW in thin ferromagnetic nanotubes. To obtain the average velocity, first, we obtained an energy expression for the continuous interfacial DMI. Secondly, we obtained the static and dynamic phase diagrams for the DW shape. Our main result shows that by delaying the Walker breakdown instability, the DW average velocity is of the order of $10^3\,\mathrm{m\,s^{-1}}$, which is greater than usual values for these systems.

2. Ferromagnetic nanotube

The system under consideration can be modeled as a ferromagnetic nanotube with an outer radius R and an inner radius βR, where $0 < \beta < 1$. The length L of the nanotube is much longer than the radius. We consider that the ferromagnetic (FM) nanotube surrounds a heavy metal material core, which leads to an interfacial DMI that is present at the interface between these two materials. The magnetization of the FM nanotube can be written as $\mathbf{M} = M_s\mathbf{\Omega}$, where M_s is the saturation magnetization and $\mathbf{\Omega}$ is an unit vector. Then, the magnetic energy functional, $\mathcal{E}$, of this system is given by

$$E[\mathbf{\Omega}] = \int dV\left[A(\boldsymbol{\nabla}\mathbf{\Omega})^2 - K(\hat{\mathbf{z}}\cdot\mathbf{\Omega})^2 + \frac{\mu_0 M_s^2}{2}(\hat{\boldsymbol{\rho}}\cdot\mathbf{\Omega})^2\right] + \int dVD\hat{\boldsymbol{\rho}}\cdot[\mathbf{\Omega}(\boldsymbol{\nabla}\cdot\mathbf{\Omega}) - (\mathbf{\Omega}\cdot\boldsymbol{\nabla})\mathbf{\Omega}], \quad (1)$$

where the right terms are the exchange, the anisotropy, the demagnetizing, and the Dzyaloshinskii–Moriya energies, respectively. A is the stiffness constant, K is the anisotropy constant, μ_0 is the vacuum permeability, and D is the interfacial Dzyaloshinskii–Moriya parameter. In particular, $D = 2D/a^2$, where D is related to the Dzyaloshinskii–Moriya vector and a is the lattice constant. We remark that the functional form of the DMI differs from the one expected in a plane geometry. This difference arises from the curvature of the system as can be appreciated in the supplementary material is available online at stacks.iop.org/NANO/31/125707/mmedia. The unit vector $\mathbf{\Omega}$, in cylindrical coordinates, can be written as

$$\begin{aligned}\Omega_\rho &= \sin\Theta(\rho,\phi,z)\cos\Psi(\rho,\phi,z),\\ \Omega_\phi &= \sin\Theta(\rho,\phi,z)\sin\Psi(\rho,\phi,z),\\ \Omega_z &= \cos\Theta(\rho,\phi,z).\end{aligned} \quad (2)$$

If we consider that the tube thickness is small ($\beta\sim 1$), the magnetization is like a vortex DW independent of the radial coordinate [20], that is,

$$\begin{aligned}\Theta(\rho,\phi,z) &= \Theta(z),\\ \Psi(\rho,\phi,z) &= \pi/2 + p,\end{aligned} \quad (3)$$

where p measures the radial component of the magnetization.

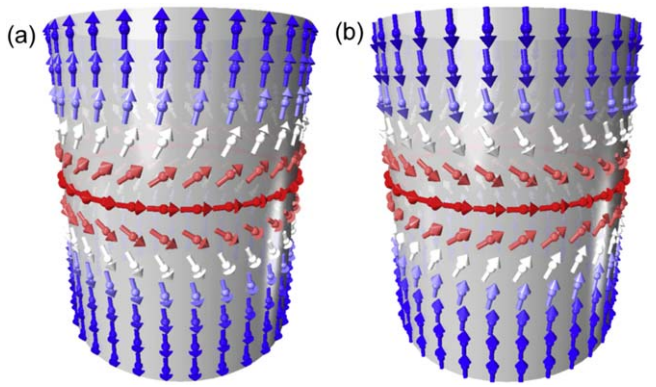

Figure 1. Magnetization for (a) $\chi = +1$ and (b) $\chi = -1$ considering $p = 0$ and neglecting Dzyaloshinskii–Moriya interaction.

Additionally, this parameter can describe the two magnetization chiralities, i.e. when $p = 0$ or $p = \pi$, there is a counterclockwise (CCW) or clockwise (CW) vortex DW, respectively. After replacing equation (3) in (2) and (1), the magnetic energy is

$$\mathcal{E} = sA\int dz\left[(\partial_z\Theta)^2 + \frac{\sin^2(\Theta)}{\lambda_p^2} - \frac{1}{W^2} + \frac{(\partial_z\Theta)}{d}\sin(p)\right], \quad (4)$$

where $s = \pi R^2(1-\beta^2)$ is the cross section area, $d = A/(2D)$, $W^2 = A/K$, and

$$\lambda_p = \left[\frac{2\log(1/\beta)}{R^2(1-\beta^2)} + \frac{\sin^2(p)}{\ell^2} + \frac{1}{dR(1+\beta)} + \frac{1}{W^2}\right]^{-1/2}, \quad (5)$$

with $\ell = \sqrt{2A/\mu_0 M_s^2}$ the exchange length, and λ_p is related to the DW length.

In our calculations, we consider a ferromagnetic material of cobalt with $\beta = 0.95$, $A = 1.3\times 10^{-11}\,\mathrm{J\,m^{-1}}$, $K = 410\,\mathrm{J\,m^{-3}}$, $M_s = 1400\times 10^3\,\mathrm{A\,m^{-1}}$, and $\ell = 3.25\,\mathrm{nm}$.

2.1. Static vortex DW

In this section, we study the magnetization equilibrium in the ferromagnetic nanotube. The equilibrium magnetic state satisfies $\partial_z\Theta = -\chi\sin\Theta/\lambda_p$, with χ taking values ± 1. The solution is

$$\cos\Theta(z) = \tanh\left(\chi\frac{z - z_0}{\lambda_p}\right), \quad (6)$$

where z_0 is the position of the DW center. We have that $\chi = +1$ means tail-to-tail magnetizations and $\chi = -1$ means head-to-head magnetizations, see figure 1.

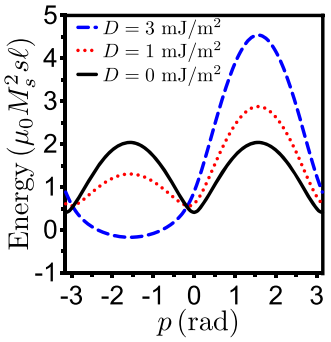

Figure 2. Total energy, normalized by $\mu_0 M_s^2 s\ell$, at zero applied field for a vortex domain wall with $\chi = -1$, as a function of the angle p for $R = 5\ell$.

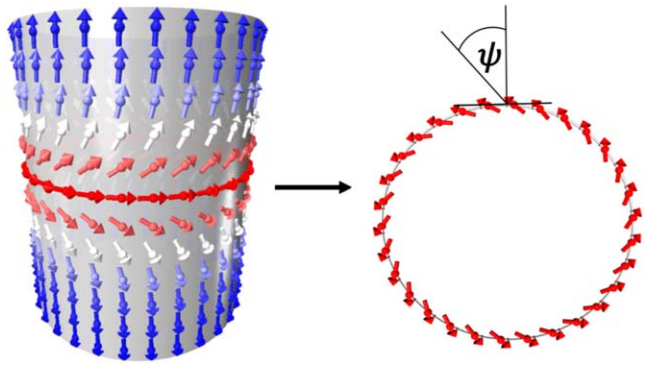

Figure 3. Magnetization for $\chi = +1$ and a top view of the magnetization at the domain wall center, when Dzyaloshinskii–Moriya interaction is included. $\psi = \frac{\pi}{2} + p$ is the angle between magnetization and the radial direction.

The total energy of the DW is up to an overall constant

$$\mathcal{E} = sA\left[\frac{4}{\lambda_p} - \chi\frac{\pi\sin(p)}{d}\right]. \tag{7}$$

We calculate the derivative of the energy with respect to p to find its optimal values. Therefore, we find the roots of the equation $\frac{\partial\mathcal{E}}{\partial p} = 0$ for p. We have that $\frac{\partial\lambda_p}{\partial p} = -\sin(p)\cos(p)\lambda_p$, then we have to solve $\frac{\partial\mathcal{E}}{\partial p} = sA[\frac{4\sin(p)\cos(p)\lambda_p}{\ell^2} + \chi\frac{\pi}{d}\cos(p)] = 0$. The solutions are $\cos(p) = 0$, i.e. $p_1 = \pi/2$ and $p_2 = -\pi/2$, and $(\frac{4\sin(p)\lambda_p}{\ell^2} + \chi\frac{\pi}{d}) = 0$, i.e.

$$p_3 = \chi\arcsin\left(\frac{\ell}{\lambda_0}\sqrt{\frac{1}{(16d^2/(\pi^2\ell^2) - 1)}}\right), \tag{8}$$

and

$$p_4 = \chi\left[\pi - \arcsin\left(\frac{\ell}{\lambda_0}\sqrt{\frac{1}{(16d^2/(\pi^2\ell^2) - 1)}}\right)\right], \tag{9}$$

where $\lambda_0 = \lambda_{p=0}$. The value of p that minimizes equation (7) depends on the value of χ and the interfacial Dzyaloshinskii–Moriya parameter.

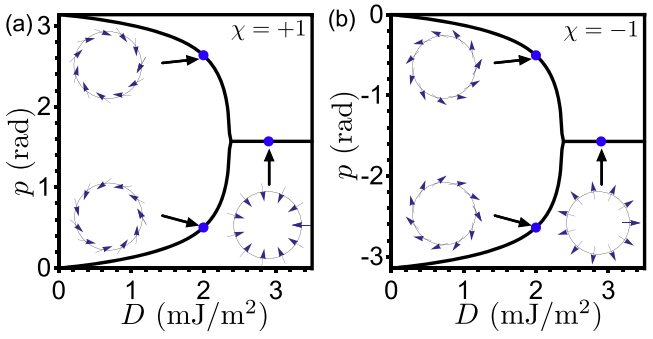

Figure 4. Value of p for the static solution, for $R = 5\ell$, as a function of D for (a) $\chi = +1$ and (b) $\chi = -1$.

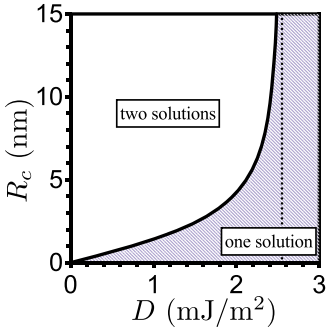

Figure 5. Static phase diagram that shows the critical radius as a function of D. For $R < R_c$ there is one static solution, while if $R > R_c$ there are two static solutions.

Figure 2 illustrates the total energy (equation (7)), normalized by $\mu_0 M_s^2 s\ell$, at zero applied field as a function of the angle p. In absence of DMI, the profile of the energy is symmetric with respect $p = 0$. We observe that for lower values of D there are two minimum and two maximum values of the energy, while for bigger values of D there are only one minimum and one maximum values of the energy. Figure 3 illustrates the schematic static vortex DW solution when the interfacial DMI is present, and figure 4 shows the values of p that minimizes the energy as a function of D with $R = 5\ell = 16.25$ nm at different χ (figure 4(a) for $\chi = +1$ and figure 4(b) for $\chi = -1$). We observe that for lower values of D there are two static solutions related to different chiralities. For $\chi = +1$, the magnetization in the DW has a component that points to the internal radial direction, while for $\chi = -1$ the magnetization has a component that points to the external radial direction. An example of the first case ($\chi = +1$) is shown in figure 3. When D increases, there is only one static solution for each χ. Then p takes $p = \pi/2$ for $\chi = +1$ (the magnetization is pointing to the internal radial direction $-\hat{\rho}$), and $p = -\pi/2$ for $\chi = -1$ (the magnetization is pointing to the external radial direction $\hat{\rho}$).

To understand the solutions of p, we need to analyze equations (8) and (9). We observe two conditions from these equations. First, if $\lambda_0 < \ell\sqrt{\frac{1}{(16d^2/(\pi^2\ell^2) - 1)}}$, the solutions p_3 and p_4 in equations (8) and (9) do not exist. Then p takes $p = \pi/2$ for $\chi = +1$, and $p = -\pi/2$ for $\chi = -1$. Therefore, for a fixed β, there is a critical external radius of the

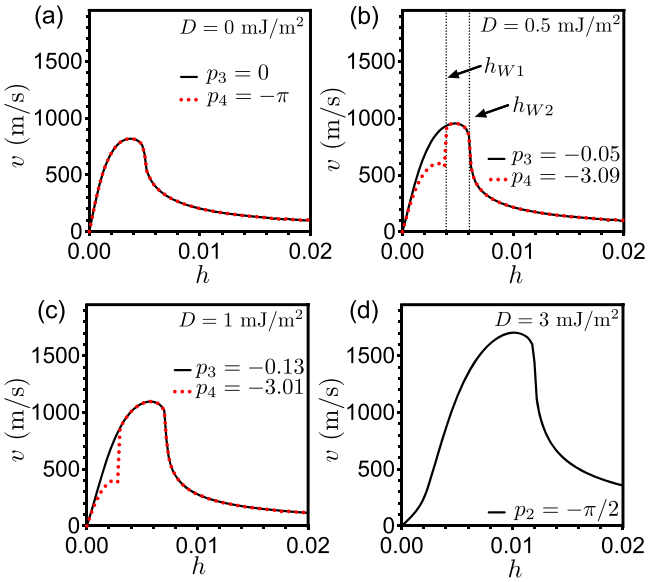

Figure 6. Velocity for $\chi = -1$ and $R = 5\ell$ as a function of the applied field for (a) $D = 0$ mJ m^{-2}, (b) $D = 0.5$ mJ m^{-2}, (c) $D = 1$ mJ m^{-2}, and (d) $D = 3$ mJ m^{-2}.

tube where there is a transition from one to two solutions of p for a specific D. The second condition is $(16d^2/(\pi^2\ell^2) - 1) > 0$ or $d > \pi\ell/4$ which is equivalent to $D < 2A/(\pi\ell) = 2.55$ mJ m^{-2}. Therefore, this condition gives an upper bound for D, i.e. if $D > 2A/(\pi\ell)$, there is only one solution for p. These two conditions can be represented in figure 5. This figure illustrates the critical radius as a function of D. If $R < R_c$, the solution is $p = \pi/2$ ($\chi = +1$) or $p = -\pi/2$ ($\chi = -1$). If $R > R_c$, there are two solutions of p, p_3 and p_4, for every χ. For $D > 2.55$ mJ m^{-2}, we observe that there is one solution for p. It is because the critical radius goes to infinity at $D = 2.55$ mJ m^{-2} (see the vertical line in figure 5).

2.2. DW motion

In this section, we study the dynamics of the vortex DW in these systems. In this case, we consider an external magnetic field applied in the axis of the ferromagnetic nanotube, $\mathbf{H} = H\hat{\mathbf{z}}$, with a Dzyaloshinskii–Moriya parameter different to zero. If we use the same procedure used to obtain the equations of motion for nanotubes without DMI [12, 21, 22], the dynamics equations for our systems are:

$$\alpha\frac{\dot{z}_0}{\lambda_p} + \dot{p} = -\chi\frac{2h}{\tau}, \tag{10}$$

$$\frac{\dot{z}_0}{\lambda_p} - \alpha\dot{p} = \frac{\sin(2p)}{\tau} - \chi\frac{\pi\ell^2}{2d\tau}\frac{\cos(p)}{\lambda_p}, \tag{11}$$

where $h = H/M_s$, $\tau = 2/(\gamma_0 M_s)$, γ_0 is the gyromagnetic ratio, and α is the damping parameter. It is convenient to write these equations as

$$\frac{\dot{z}_0}{\lambda_p} = -\frac{2\chi\alpha}{\tau(1+\alpha^2)}\left(h - \frac{h^*(p)}{\alpha}\right), \tag{12}$$

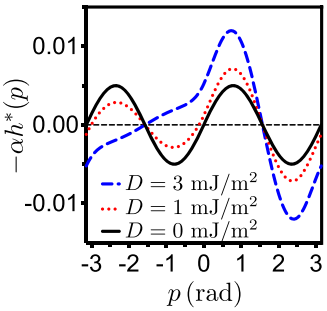

Figure 7. Field $-\alpha h^*(p)$ for a vortex domain wall, with $\chi = -1$, as a function of the angle p for $R = 5l$.

$$\dot{p} = -\frac{2\chi}{\tau(1+\alpha^2)}(h + \alpha h^*(p)), \tag{13}$$

where

$$h^*(p) = \frac{\chi\sin(2p)}{2} - \frac{\pi\ell^2}{4d}\frac{\cos(p)}{\lambda_p} \tag{14}$$

is an effective field which is proportional to the derivative of the energy $\mathcal{E}$ with respect to p. Figure 6 illustrates the average velocity of the DW, $v = \langle\dot{z}_0\rangle$, as a function of the normalized applied field for different values of the Dzyaloshinskii–Moriya parameter, specifically, in figure 6(a) $D = 0$ mJ m^{-2}, in figure 6(b) $D = 0.5$ mJ m^{-2}, in figure 6(c) $D = 1$ mJ m^{-2}, and in figure 6(d) $D = 3$ mJ m^{-2}. In these figures we consider $\chi = -1$ and $R = 5\ell$. If $\chi = +1$, we obtain the same magnitudes for the velocity, which is negative. In the case for $\chi = +1$ the propagation of the DW is in the direction $-\hat{z}$ (opposite to the applied field) while for $\chi = -1$ the propagation of the DW is in the direction $\hat{z}$ (in the same direction of the applied field).

First, by increasing D, we observe an enhancement of the maximum DW average velocity. Also, for $D = 0$, we observe the same curve proposed by Landeros and Núñez for the two initial conditions of p [12]. However, for $D = 0.5$ mJ m^{-2} and $D = 1$ mJ m^{-2} (see figures 6(b) and (c), respectively), we observe two different curves depending on the initial condition of p. For $p = p_3$, we have the same behavior of $D = 0$. But for $p = p_4$, there is a drop of the average velocity at h_{W1}, see figure 6(b). Similar behavior was observed in the article of Landeros and Núñez when the total energy of the system has the exact demagnetization energy. Finally, when we increase the Dzyaloshinskii–Moriya parameter (see figure 6(d)), there is only one static solution that evolves in the same way as $D = 0$. In the supplementary material, there are three animations of the DW dynamics corresponding to figure 6(b) for $h = 0.0035$, 0.005, and 0.008.

2.3. Walker critical field and maximum velocity

To understand well figure 6, it is necessary to calculate the Walker fields, h_{W1} and h_{W2}, and the critical DW average velocity. The Walker fields, h_{W1} and h_{W2}, are obtained

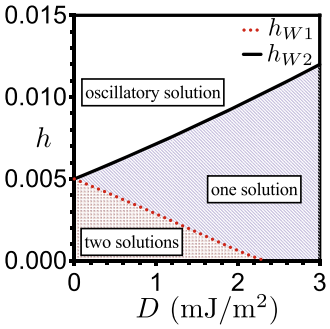

Figure 8. Dynamic phase diagram that shows the Walker fields, for $R = 5\ell$, as a function of D. There are different dynamic solutions.

through the condition $\dot{p} = 0$ in equation (13), i.e.

$$h = -\alpha h^*(p) \Rightarrow h = \frac{\alpha}{2}\left[\frac{\pi\ell^2}{2d\lambda_p} - 2\chi\sin(p)\right]\cos(p). \quad (15)$$

Then, we need to obtain the values of p that satisfies this equation for the maximum values of h, i.e. $dh^*(p)/dp = 0$, and the energy must be minimum for the solutions of p. Figure 7 shows the field $-\alpha h^*(p)$ as a function of the angle p for $\chi = -1$. We observe that for $D < 2.55\ \mathrm{mJ\,m^{-2}}$ there are two maximum (h_{W1} and h_{W2}, with $h_{W1} < h_{W2}$), while for $D > 2.55\ \mathrm{mJ\,m^{-2}}$ there is one maximum (h_{W2}). For a positive external applied field we observe different behaviors. There are three external applied field regions for $D < 2.55\ \mathrm{mJ\,m^{-2}}$: (i) $0 < h < h_{W1}$, (ii) $h_{W1} < h < h_{W2}$, and (iii) $h > h_{W2}$. In the first region, (i), there are four roots of equation (14) where two of them have the lowest energies and represent the new values of p for each initial condition. These initial conditions are related with two chiralities (CCW) and (CW). The applied field does not deliver enough energy to the system to exceed the energy barriers observed in figure 2. Then, the two initial chiralities are preserved and the DW motion evolves to a constant velocity and a new equilibrium angle, which are different for each chirality. In the second region, (ii), there are two solutions of p, where only one solution has the minimum energy and gives the value of p that evolves from the two initial conditions. Then for $h = h_{W1}$, we observe a drop in the velocity. It is because one of the initial conditions evolves to the other because the applied field delivers enough energy to the system to exceed one of the energy barriers observed in figure 2. Then the system increases its velocity for this chirality with the purpose to minimize its energy. In the last region, (iii), there are not solutions for p and we observe an oscillatory solution for this variable. We can conclude that the term associated to the DMI introduces a chiral asymmetry in the vortex DW propagation. Therefore, the DW velocity depends on the initial chirality of the system.

Figure 8 illustrates the magnitude of the Walker fields, h_{W1} and h_{W2}, as a function of D for $R = 5\ell$ at fixed β. This figure shows the dynamic phase diagram of the solutions of p. From this figure, we observe that there are three possibilities for the solutions of p if $D < 2A/(\pi\ell) = 2.55\ \mathrm{mJ\,m^{-2}}$ (one dynamics solution, two dynamics solutions, and oscillatory solutions of p) and two possibilities for the solution of p if

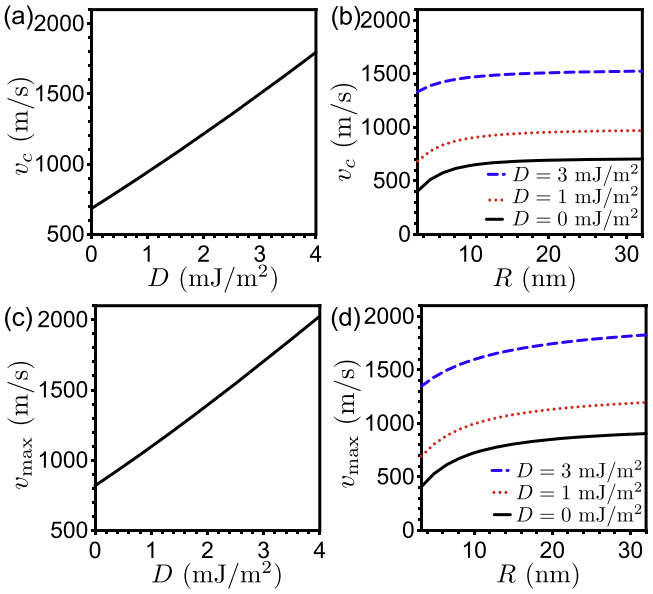

Figure 9. (a) Critical velocity as a function of D for $R = 5\ell$ and $\chi = -1$, and (b) critical velocity as a function of R for different values of D.

$D > 2A/(\pi\ell) = 2.55\ \mathrm{mJ\,m^{-2}}$ (one dynamics solution and oscillatory solutions of p). In addition, we observe that both Walker fields have approximately linear behavior at low values of D, where h_{W1} decreases and h_{W2} increases as D increases.

From figure 6, we observe an enhancement of the critical average velocity and the maximum average velocity of the DW when we change the Dzyaloshinskii–Moriya parameter. The critical velocity of the DW, v_c, is obtained at the Walker field h_{W2}, i.e. $v_c = v(h_{W2})$. From equation (10), v_c is given by

$$v_c = 2\frac{h_{W2}}{\alpha}\frac{\lambda_{p'}}{\tau}, \quad (16)$$

where p' is the dynamics solution of p at $h = h_{W2}$. Additionally, the maximum average velocity of the DW, $v_{\max}$, is obtained through the condition $dv/dh = 0$. Figure 9 illustrates the critical average velocity and the maximum average velocity of the DW as a function of D and R. From these figures, we observe that the average velocities increases when we increase D and R. In our system, the maximum average velocity is of the order of $10^3\ \mathrm{m\,s^{-1}}$. Due to the fact that the DMI introduces a chiral asymmetry in the vortex DW propagation, as we can observe in figure 7, a larger external field is necessary (if we compare with $D = 0$) to reach the Walker breakdown instability. This delay is reflected in an increase of the speed. In other words, our system gives a fast DW motion for ferromagnetic materials when the interfacial DMI is present.

3. Conclusions

We studied the DWs dynamics in thin ferromagnetic nanotubes when the interfacial DMI is present. We observed an ultrafast DW average velocity of the order of $10^3\ \mathrm{m\,s^{-1}}$. Also, we obtained static and dynamic phase diagrams for the shape

of the DW, p value, depending on the Dzyaloshinskii–Moriya parameters. The static phase diagram shows that if $D \geqslant 2A/(\pi\ell)$, the magnetization of the DW points completely along the radial direction. In the other case, if $D < 2A/(\pi\ell)$, the DW has two possible chiralities. In the dynamic phase diagram, we observed two Walker fields, h_{W1} and h_{W2}, where the first one corresponds when the average velocity is independent of the chirality in the stationary DW motion, and the second one when the DW starts to have oscillatory motion. The remarkable velocities achieved through this configuration could greatly benefit the development of spintronic devices.

Acknowledgments

We acknowledge financial support in Chile from FONDECYT 1161018, 1190324 and Financiamiento Basal para Centros Científicos y Tecnológicos de Excelencia FB 0807. D.M.-A. acknowledges Postdoctorado FONDECYT 2018, folio 3180416.

ORCID iDs

S Allende https://orcid.org/0000-0002-6138-6862

References

[1] Sheka D D, Kravchuk V P and Gaididei Y 2015 *J. Phys. A: Math. Theor.* **48** 125202
[2] Streubel R, Fischer P, Kronast F, Kravchuk V P, Sheka D D, Gaididei Y, Schmidt O G and Makarov D 2016 *J. Phys. D: Appl. Phys.* **49** 363001
[3] Hertel R 2013 *SPIN* **03** 1340009
[4] Gaididei Y, Kravchuk V P and Sheka D D 2014 *Phys. Rev. Lett.* **112** 257203
[5] Otálora J A, Yan M, Schultheiss H, Hertel R and Kákay A 2016 *Phys. Rev. Lett.* **117** 227203
[6] Thiaville A, Nakatani Y, Miltat J and Suzuki Y 2005 *Europhys. Lett.* **69** 990
[7] Mougin A, Cormier M, Adam J P, Metaxas P J and Ferré J 2007 *Europhys. Lett.* **78** 57007
[8] Yan M, Kákay A, Gliga S and Hertel R 2010 *Phys. Rev. Lett.* **104** 057201
[9] Hertel R 2016 *J. Phys.: Condens. Matter* **28** 483002
[10] Carvalho-Santos V, Elias R, Altbir D and Fonseca J 2015 *J. Magn. Magn. Mater.* **391** 179–83
[11] Kravchuk V P, Sheka D D, Kákay A, Volkov O M, Rößler U K, van den Brink J, Makarov D and Gaididei Y 2018 *Phys. Rev. Lett.* **120** 067201
[12] Landeros P and Núñez A S 2010 *J. Appl. Phys.* **108** 033917
[13] Otálora J, López-López J, Landeros P, Vargas P and Nunez A 2013 *J. Magn. Magn. Mater.* **341** 86–92
[14] Thiaville A, Rohart S, Jué É, Cros V and Fert A 2012 *Europhys. Lett.* **100** 57002
[15] Jué E *et al* 2016 *Phys. Rev.* B **93** 014403
[16] Thai H P *et al* 2016 *Europhys. Lett.* **113** 67001
[17] Goussev A, Robbins J M, Slastikov V and Tretiakov O A 2016 *Phys. Rev.* B **93** 054418
[18] Bae C, Shin H and Nielsch K 2011 *MRS Bull.* **36** 887–97
[19] Chong Y T, Görlitz D, Martens S, Yau M Y E, Allende S, Bachmann J and Nielsch K 2010 *Adv. Mater.* **22** 2435–9
[20] Landeros P, Allende S, Escrig J, Salcedo E, Altbir D and Vogel E E 2007 *Appl. Phys. Lett.* **90** 102501
[21] Duine R A, Núñez A S and MacDonald A H 2007 *Phys. Rev. Lett.* **98** 056605
[22] Duine R A and Stoof H T C 2001 *Phys. Rev.* A **65** 013603